Applied Catalysis B: Environmental 96 (2010) 577–585

Contents lists available at ScienceDirect

Applied Catalysis B: Environmental

journal homepage: www.elsevier.com/locate/apcatb

The effect of particle shape on the activity of nanocrystalline TiO_2 photocatalysts in phenol decomposition. Part 3: The importance of surface quality

K. Mogyorósi [a], N. Balázs [a], D.F. Srankó [a], E. Tombácz [b], I. Dékány [b], A. Oszkó [b], P. Sipos [a,*], A. Dombi [a]

[a] Department of Inorganic and Analytical Chemistry, University of Szeged, Research Group of Environmental Chemistry, ReGECh Szeged, H-6701, P.O. Box 440, Hungary
[b] University of Szeged, Department of Physical Chemistry and Material Science, Aradi Vt. 1, H-6720 Szeged, Hungary

ARTICLE INFO

Article history:
Received 25 November 2009
Received in revised form 1 March 2010
Accepted 3 March 2010
Available online 9 March 2010

Keywords:
Titania
Anatase
Rutile
Nanoparticles
Phenol decomposition
Heterogeneous photocatalysis
Flame hydrolysis
Shape dependence
Dynamic light scattering
Isoelectric point
X-ray photoelectron spectroscopy
Oxygen consumption
Complete mineralization
Aromatic intermediates

ABSTRACT

Bare TiO_2 photocatalysts made up of polyhedral nanoparticles have been prepared by flame hydrolysis. In order to obtain deeper understanding of the interplay between the properties determining the photocatalytic performance, surface, aggregation and photocatalytic properties have been analyzed and compared. The aggregation of nanoparticles in aqueous solution of NaCl was determined by dynamic light scattering (DLS) technique. The average hydrodynamic diameters of the aggregates investigated under environmentally relevant conditions do not differ significantly in the pH range of 5–6. Zeta potential measurements were also done during DLS analysis, which revealed remarkably low pH_{IEP} values for our flame made samples comparing to the commercial titanias. Furthermore an explicit correlation between the isoelectric points and the synthesis parameters was revealed. O 1s XP spectra for the high activity samples were also recorded and interpreted. Oxygen consumption experiments were used to test the photocatalytic activity in suspensions. The method was found to be not only rapid and inexpensive but also reasonably reproducible. Normalizing the oxygen consumption rate with the specific surface area of the sample and the concentration of the suspension, a good correlation could have been found with the traditionally determined photocatalytic activity. HPLC measurements were used to study the degradation mechanism of phenol via determining the concentration profile of various dihydroxy intermediates, i.e., hydroquinone (HQ) and pyrocatechol (PC). The quality of the photocatalyst strongly affects the maximum ratio of HQ:PC during the photocatalytic degradation process. For our catalysts higher pyrocatechol concentrations were measured than for Degussa P25. TOC measurements were used to follow the complete mineralization. Using our best photocatalysts (e.g., anatase:rutil ratio of 82:18 and mostly polyhedral particles, with 21 m^2/g BET surface area), phenol concentration decreased faster than for P25, however, the mineralization rate was somewhat lower. This can be attributed to the lower adsorption capacity of our polyhedral particles against PC and carboxylate containing intermediates formed during the more advanced stages of decomposition. These data elucidate, that hydrophilicity, O_2-consumption properties and adsorption/complexation of the target compounds and their degradation products are equally important parameters in determining the photocatalytic performance of catalysts, which otherwise possess similar material properties.

1. Introduction

The optimization of synthesis parameters of flame made titanium dioxide nanoparticles were reported in the first two parts of this series [1,2]. Spherical and polyhedral particles were produced in two different homemade burners in our diffusion flame reactor. Degussa P25 TiO_2 (P25 in the followings), which is also produced via a similar synthesis method, is the most efficient photocatalyst in the decomposition of the majority of organic compounds, relative to other commercially available photocatalysts [3]. The complete mineralization of 2-chlorophenol was observed at sufficiently high rate, when we used this reference photocatalyst in our studies [4–6]. However, P25 was found to be less efficient for compounds like carboxylic acids [3,7,8]. Clearly, it is rather important to understand the underlying reasons of this substrate specificity.

It was concluded in the first part of the present study that otherwise similar particles are more active photocatalytically if they have mostly polyhedral shape instead of spherical one. Besides the traditionally investigated structural (or material) parameters, such as particle size [9–11] and phase composition [12,13], the surface properties of the photocatalysts are also expected to be crucially important parameters. For example, the hydrophilicity can be followed by studying the level of aggregation in water as it was demonstrated in Refs. [9,14,15]. This parameter is mainly

* Corresponding author. Tel.: +36 62 544 338; fax: +36 62 420 505.
E-mail address: sipos@chem.u-szeged.hu (P. Sipos).

0926-3373/$ – see front matter © 2010 Elsevier B.V. All rights reserved.
doi:10.1016/j.apcatb.2010.03.007

determined by the OH-group density on the surface, which can be determined by XPS technique [16–19].

The characterization of the photocatalysts is usually carried out by photocatalytic tests for a single model substrate (or, at most, for a limited number of them). Naturally, this approach cannot reveal the full photocatalytic potential of a given photocatalyst. Studying the formation of intermediates and the decrease in the total organic carbon content (TOC) could provide a chance to better understand the working mechanism of our materials. Intermediate studies are found in the literature for photocatalytic decomposition of phenolic compounds [5–7,20–29]. Dihydroxy (such as hydroquinone (HQ) and pyrocatechol (PC)), trihydroxy aromatic and carboxylic acid intermediates were found to be formed during the complete mineralization of phenols. Besides the adsorption of the substrate, the surface complexation of these intermediates also strongly influences the rate of complete mineralization.

During the photocatalytic process, adsorption of water, molecular oxygen and the substrate takes place. The hydrophilicity affects the adsorption of water on the surface of titania. The specific surface area influences mostly the adsorbed amount of well-adsorbing substrates (e.g., salicylic acid), therefore the higher surface area is beneficial for the photocatalytic decomposition of such compounds [30–34]. The oxygen adsorption on titanium dioxide was studied by Chhor et al. [35] in gas phase and solution phase as well. They found that the rate of oxygen consumption in irradiated suspensions is a good indicator of the photocatalytic activity of the applied photocatalysts.

To extend our knowledge on the interrelations between surface quality and photocatalytic performance, selected flame made samples were examined in this part of our studies. We have attempted to characterize their aggregation behaviour in aqueous phenol solution and their pH-dependent surface charge formation by DLS technique, and to investigate their surface by XPS method. Furthermore, oxygen consumption experiments, intermediate studies and TOC measurements have been used to characterize the full photocatalytic potential of these photocatalysts.

2. Experimental

2.1. Synthesis of the photocatalysts

Titanium dioxide samples were prepared in home made co-flow diffusion flame reactors equipped with bubble vapour generators and with two, slightly different burners (Burner A and B, for detailed technical description see. Ref. [2]). The synthesis is based on the introduction of titanium(IV) chloride vapour into a hydrogen-air flame, in which the rapid hydrolysis and crystallization occur. The titania aerosol thus formed was collected in a condenser. The suspension thus obtained was washed by dialysis and the product was dried. During the synthesis, the flow rates of the various gases employed were separately controlled.

Samples are indicated by a letter referring to the burner, has been used during their synthesis and by numbers describing the flame conditions [2]. This numbering has been followed in constructing Tables 1 and 2, where sample codes indicating the synthesis parameters used during sample preparation are also shown. These codes contain the type of the burner, the hydrogen–oxygen molar ratio, the precursor vapour feeding rate in mL/min and the temperature of the liquid precursor under bubbling in °C (all sepa-

Table 1
Material properties and photocatalytic performance of the TiO_2 photocatalysts studied. Sample codes in the first column contain the type of the burner, the hydrogen–oxygen molar ratio, the precursor vapour feeding rate in mL/min and the temperature of the liquid precursor under bubbling in °C.

Sample number (Sample code)[a]	F[b] (%)	A:R[c]	d_{TEM}[d] (nm)	$a^{S_{BET}}$[e] (m^2/g)	d_{DLS}[f] (nm)	pH_{IEP}[f] (10 mM NaCl)	$r_{0,phenol}$[g] (10^{-8} M/s)	Normalized $r_{0,phenol}$[h] (10^{-9} mol s^{-1} m^{-2})
B-1.00-355-30	100	96:4	38	45	570	3.5	15.6	3.5
B-1.24-355-30	96	82:18	69	21	550	2.5	25.7	12.2
B-1.41-355-30	90	57:43	77	19	690	2.2	9.8	5.2
B-1.24-178-30	95	80:20	61	24	–	–	21.4	8.9
B-1.24-710-30	97	84: 16	59	27	640	2.9	20.8	7.7
B-1.24-355-70	97	81:19	72	22	580	3.8	19.4	8.8
P25 B	100	89:11	26	50	900	6.0	15.4	3.1

[a] The numbers within the code carry information on the preparation conditions of the specimen; for more details see Section 2 and Ref. [2].
[b] Frequency of polyhedral particles.
[c] Anatase to rutile ratio.
[d] Average particle diameter obtained from TEM measurements.
[e] Specific surface area from N_2 adsorption.
[f] Average diameter of the aggregates obtained from DLS measurements and IEP values determined in solutions with c_{NaCl} = 10 mM and c_{TiO_2} = 10 mg/L.
[g] Initial rate of phenol decomposition as defined in Section 2.
[h] $r_{0,phenol}/(a^{S_{BET}} \times \text{catalyst loading})$.

Table 2
Photocatalytic properties of the TiO_2 photocatalysts studied and the concentration of hydroquinone and pyrocatechol during the decomposition of phenol.

Sample number (sample code)[a]	$r_{0,phenol}$[b] ($\times 10^{-8}$ M/s)	r_{0,O_2}[c] ($\times 10^{-8}$ M/s)	$r_{0,O_2}/r_{0,phenol}$	c_{max}^{HQ}[d] ($\times 10^{-5}$ M)	c_{max}^{PC}[e] ($\times 10^{-5}$ M)	$c_{max}^{HQ}/c_{max}^{PC}$
B-1.00-355-30	15.6	29.4	1.88	6.9	3.0	2.30
B-1.24-355-30	25.7	28.9	1.12	7.7	5.2	1.48
B-1.41-355-30	9.8	5.9	0.60	7.2	6.4	1.13
B-1.24-178-30	21.4	28.2	1.32	8.0	4.1	1.95
B-1.24-710-30	20.8	24.9	1.20	5.2	4.3	1.21
B-1.24-355-70	19.4	22.3	1.15	7.7	6.8	1.13
P25 B	15.4	31.6	2.05	6.6	1.5	4.40

[a] The numbers within the code carry information on the preparation conditions of the specimen; for more details see Section 2 and Ref. [2].
[b] Initial reaction rate of phenol decomposition.
[c] Oxygen consumption rate according to the definition given in Section 3.
[d] Maximum concentration of hydroquinone (HQ) during the photocatalytic degradation of phenol.
[e] Maximum concentration of pyrocatechol (PC) during the photocatalytic degradation of phenol.

rated by hyphens, for example: B-0.96-148-30). The present paper focuses on the investigation of the properties of selected polyhedral particles prepared with burner B and some samples also made using burner A.

2.2. Characterization of the photocatalysts

Characterization of the samples' material properties has been described in details in our previous publication [1]. Briefly X-ray diffraction (XRD) measurements were performed on a *Rigaku* diffractometer. The average diameters of the particles were obtained by means of the *Scherrer* equation. The weight fraction of anatase and rutile was calculated for each sample. Transmission electron microscopic (TEM) studies were performed to characterize the particle size and size distribution and also to observe the morphology of the particles. TEM micrographs were recorded on a *Philips CM* 10 instrument operating at 100 kV using *Formvar* coated copper grids. The specific surface area of the catalysts was determined by nitrogen adsorption at 77 K by a *Micromeritics* gas adsorption analyzer (*Gemini Type* 2375). The specific surface area was calculated using the BET method. The results of these structural investigations have been published in details in the first two parts of this series [1,2].

Dynamic light scattering (DLS) measurements were performed using a *NanoZS* apparatus (Malvern, UK) operating at $\lambda = 633$ nm produced by a He–Ne laser (4 mW), operating in backscattering mode at angle 173°. The zeta potential and hydrodynamic size values were measured at 25 ± 0.1 °C in a disposable zeta cell (DTS 1060). Particles from the stock suspensions were dispersed in 0.01 M indifferent electrolyte (NaCl) solutions to set 10 mg/L solid content. The pH of dilute suspensions were adjusted in the range of 2–10 and measured before a sample was placed in the cell. The average values of zeta potential as well as hydrodynamic diameter calculated from 3rd order cumulant fits of the correlation functions measured at a given kinetic stage are presented. During the experiments TiO_2 samples were dispersed in NaCl (0.01 M) aqueous solutions. The obtained stock suspensions ($c_{TiO_2} = 1$ g/L) were then diluted to the concentration of 10 mg/L for ensuring an optimal detectable light intensity. The pH of the dispersions was adjusted using NaOH and HCl-solutions of analytical grade and they were kept for a couple of hours prior to the measurement in order to achieve the natural equilibrium. In a typical experiment a small portion (~3 mL) was agitated again and ultrasonicated for 10 s before placing it into the sample holder. The suspension was kept in the instrument for about 1 min and after this waiting period the measurement was started.

X-ray photoelectron spectra of selected samples were taken with a *SPECS* instrument equipped with a *PHOIBOS* 150 *MCD* 9 hemispherical electron energy analyzer operated in the FAT mode. The excitation source was the Kα radiation of a magnesium anode ($h\nu = 1253.6$ eV). The X-ray gun was operated at 180 W power (12 kV, 15 mA). The pass energy was set to 20 eV, the step size was 25 meV, and the collection time in one channel was 150 ms. Typically five scans were added to get a single spectrum. The C 1s binding energy of adventitious carbon was used as energy reference: it was taken 285.1 eV. With this method Ti $2p_{3/2}$ spectra were detected at 459 ± 0.2 eV corresponding to Ti^{4+}. For data acquisition both manufacturers (*SpecsLab*2) and commercial (*CasaXPS*, *Origin*) software were used. Before the data analysis X-ray satellites originating from the non-monochromatic excitation source were removed from the spectra.

2.3. Determination of the photocatalytic activities

The performance of the catalysts prepared was characterized by using the photocatalytic decomposition of phenol in solution. Details of the setup have been published elsewhere [1]. The photoreactor (100.0 mL) was an open tube with double walls, surrounded by a thermostating jacket (25.0 ± 0.1 °C). The continuously stirred reactor was surrounded and irradiated by six fluorescent lamps (6 W power, radiation maximum at 365 nm). The concentration of phenol and its main aromatic intermediates, such as HQ and PC were measured with an HPLC system consisting of a *Merck-Hitachi L*-7100 low-pressure gradient pump equipped with a *Merck-Hitachi L*-4250 UV–VIS detector and a *Lichrospher RP* 18 column applying methanol/water mixture as eluent. The initial concentration of the substrate was 5.0×10^{-4} M. 1 g/L photocatalyst concentration was used throughout. Samples were taken from the suspension in predetermined time intervals, for 120 min.

The complete mineralization was followed by measuring the total organic carbon (TOC) content in the solutions. The measurement was carried out in a *Euroglas TOC* 1200 apparatus (Delft, The Netherlands). The TOCs of solutions were determined directly by injecting samples of 100 μL, combusted at 1000 °C in an oxygen–argon mixture and the produced CO_2 was analyzed. Standard solutions of oxalic acid were used for calibration.

The initial rate of the photocatalytic degradation of the model compounds, r_0 was considered to be the measure of the efficiency of a given photocatalyst. To determine r_0, an empirical function was fitted to the experimentally observed $c = f(t)$ data points. If the fitting yielded satisfactory description for the data then the slope of the empirical function at $t = 0$ yields the initial rate of the photocatalytic reaction.

The photocatalytic activity was also studied by continuously measuring the oxygen consumption in the irradiated suspensions containing phenol ($c_{0,phenol} = 0.5$ mM, $c_{TiO_2} = 200$ mg/L). The suspension was equilibrated by air via purging and then sealed in a reactor before the irradiation started. The dissolved oxygen analyzer is equipped with a biamperometric cell (*Consort C*835), which was immersed in the sealed system thus the oxygen consumption of photocatalytic reactions could have been monitored directly during irradiation. The sealed photoreactor employed was basically identical with that reactor used for the general photocatalytic experiments [1–2], except that this reactor is equipped with two inlets: one for bubbling and another to hold the oxygen detecting electrochemical cell. During a typical experiment, the larger portion of the suspension (95 mL) containing phenol is placed in the reactor and air is bubbled throughout for about 10 min to saturate the suspension with O_2. After equilibration, and at atmospheric pressure, the concentration of O_2 is about 8.25 ppm for 25.0 °C. The reactor is thermostated for 25.0 ± 0.1 °C. The measuring cell has been calibrated prior to each measurements with aerated MilliQ water. When the concentration of the dissolved oxygen becomes stable at 8.25 ppm, the smaller portion of the suspension (5 mL) is finally placed into the reactor and it is immediately closed with a glass plug at the open joint. This way the reactor is now completely sealed, having only a negligible ($V_{air} < 0.5$ mL) gas phase inside at the upper part of the reactor. Finally the UV lamps are switched on and the decrease of the dissolved oxygen concentration is monitored.

The response time of the cell was tested via keeping it in aerated distilled water until stable reading and then suddenly placing it into distilled water purged with nitrogen. The drop of the displayed oxygen concentration was monitored and we found that it dropped to 10% of the original (<1 mg/L) within 45 s. Accordingly, the test conditions were optimized in order to keep in mind the response time. The concentration of the suspension was therefore decreased from the usual 1.0 g/L to 0.2 g/L, in order to slow down the rate of the oxygen consumption.

3. Results and discussion

3.1. Material properties of the selected photocatalysts

The material properties of the selected samples are summarized in Table 1. These samples contain mostly polyhedral particles (90–100%) mainly in anatase form (80–96 wt%). There is only one sample with relatively high rutile content (B-1.41-355-30, 43 wt%). The average particle diameter data determined by TEM micrographs are also listed in Table 1, it was found to be in the range of 38–77 nm. The specific surface area values of these materials are between 19 and 45 m^2/g, depending on the conditions applied during the synthesis. The photocatalytic activity was found to be the highest for sample B-1.24-355-30. The calculated initial decomposition rates for phenol, $r_{0,phenol}$, are also shown. The normalized reaction rates are calculated by dividing r_0 values by the measured specific surface area and the titanium dioxide loading. This latter parameter indicates the photocatalytic quality of the surface.

On the basis of TEM images (beside the diameter of the individual particles, which is one of the most important parameters to describe a sample's property) the size distribution and the frequency of the polyhedral particles in the selected samples have been determined (Fig. 1 and Table 1). The polydispersity of the samples investigated is similar. There is only one sample with significantly smaller particles than the others (B-1.00-355-30, d = 38 nm). It should be noted here that the material properties of this particular sample is rather similar to that of P25 B reference sample (P25 B name was given in our previous publications for the P25 sample having higher anatase content, 89 wt% than the other P25 sample with 79 wt% anatase content, which was called P25 A [1]).

3.2. Dynamic light scattering: particle size and IEP measurements

The crucial parameters determining the efficiency of excitation are the optimum crystal size, the phase composition and the level of aggregation in the solution. The colloidal stability of the aqueous

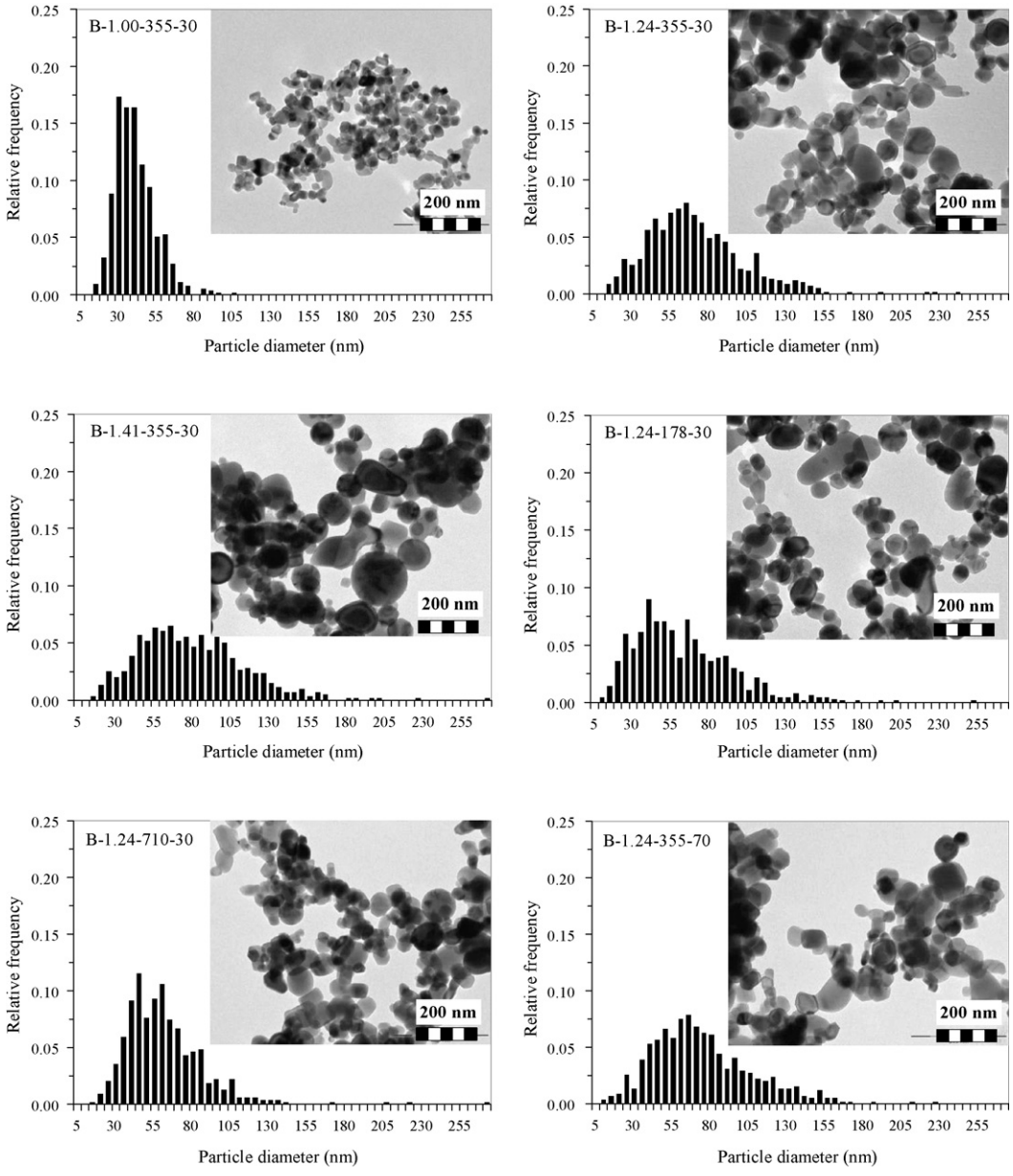

Fig. 1. Size distribution and TEM images of samples prepared by burner B (from Table 1).

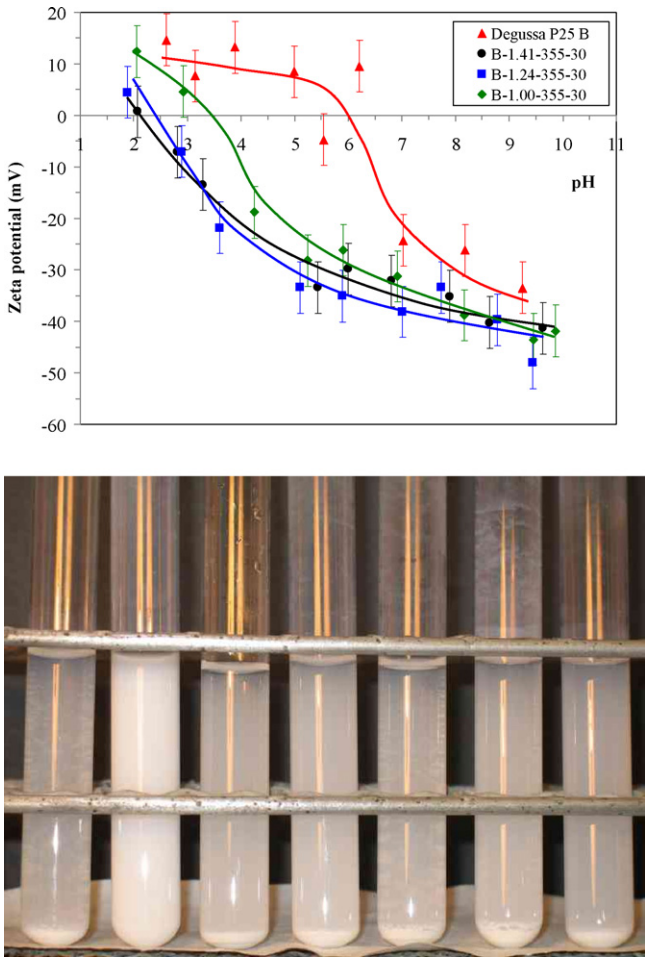

Fig. 2. Zeta potentials under various pH values in aqueous suspensions of three selected samples (c_{TiO_2} = 10 mg/L, c_{NaCl} = 10 mM). The test tubes contain aqueous suspensions of the samples (from the left to the right, in the same order as listed in Table 1). The suspensions contain NaCl (10 mM), c_{TiO_2} = 1 g/L and sedimentation time was 60 min.

titanium dioxide dispersions mainly depends on the hydrophilicity (thus on the density of surface hydroxyl groups) of the particles, the particle size, the pH and the ionic strength of the solution. Smaller aggregate size provides better light absorption since larger portion of the particles can be excited being exposed directly to the irradiating light. The aggregation certainly increases the number of particles shadowed by the surrounding particles in the outer layer of the aggregate. Flame made titanium dioxide samples such as P25 are well known to be very hydrophilic. They are easily dispersed in water and form stable acidic suspensions, in which the particles do not settle even after several days.

The surface charge of the particles has an effect not only on aggregation processes but influences the adsorption of different compounds as well, especially those with ionic form. Due to electrostatic attraction or repulsion phenomena it could be a determining factor of whether the molecules can react directly on the catalyst surface or interact with radicals released by that into the aqueous medium [36]. For this reason it is worth having information about the pH dependence of both charging and aggregation behaviour of catalyst particles. By the aid of the applied DLS technique it was possible to measure zeta potential and aggregate size simultaneously.

Fig. 2 shows the pH dependence of zeta potentials in the case of three different flame made samples and P25 B. The sign of these potentials is the same as that of the excess charge of particle moving together with the adhered layer of counterions, and its magnitude is somewhat proportional to the particle charge. The sign of the zeta potentials measured in the metal oxide dispersions reverses at a characteristic pH, where these amphoteric particles do not hold excess charge. It can be identified as the pH of isoelectric point (IEP) [37]. As seen the measured zeta potential values decreased with increasing pH for each sample and the sign reversal of zeta potentials occurred at different pHs; significantly smaller IEP values, such as 2.0–3.5 were determined for our samples compared to the IEP of P25 ($pH_{IEP} \sim 6$, that is close to the average IEP of a titanium dioxide sample (5.6) [38]). The IEP values of our flame made samples decreased gradually from pH 3.5 to 2.0 as the hydrogen–oxygen molar ratio increased during the preparation of titania photocatalysts. The lowest IEP was found for a sample that was made in a highly reducing atmosphere, resulting in bluish color that most likely indicates the presence of a very small amount of Ti^{3+} in the crystal structure. The presence of Ti^{3+} instead of the stoichiometric Ti^{4+} obviously altered not only the photocatalytic activity (through creation of oxygen vacancies) but also the surface charge state, therefore the IEP of titania particles. The significant shift of IEP to the acidic region may predict a good catalytic performance of our samples, since Gumy et al. [36] found that photocatalysts with low IEP (<3) were the most active photocatalysts decomposing phenol. Note, that based on the test tube series on Fig. 2, the most active sample (B-1.24-355-30) displays the highest colloid stability (i.e., second test tube from the left) and (based on the data shown in Table 1) the best sample has the smallest hydrodynamic diameter (d_{DLS}).

Table 1 indicates the hydrodynamic diameter of the aggregates in the suspensions made from the selected flame made samples and from P25 B. These materials are very hydrophilic, sedimentation was noticed only in few instances within several hours in water. Naturally, the presence of NaCl in the dispersions induces aggregation of particles. The average hydrodynamic diameter values of aggregates are between 550 and 690 nm that are significantly smaller that that determined for P25 B (D = 900 nm) in dilute aqueous dispersions at pH ~ 6. Suspension made of sample B-1.24-355-30 showed the highest colloidal stability and the smallest aggregate size (550 nm). If the pH is lower than the IEP value then the particles are positively charged due to the protonation of the surface OH-groups and therefore stabilized against aggregation by electrostatic repulsion. Similar stabilization occurs at higher pH values, except that when the pH is higher than the IEP then the particles are negatively charged due to the de-protonation of the surface OH-groups. One would expect that the smallest hydrodynamic diameter results in the highest photocatalytic activity. The highest phenol decomposition activity was found for the sample prepared at 1.24 hydrogen–oxygen molar ratio. It should be emphasized here that the sample prepared at 1.41 hydrogen–oxygen molar ratio contained significantly higher rutile content than the other samples possibly due to the higher flame temperature or due to the presence of Ti^{3+} ions in the lattice. The lower anatase content obviously lowered the catalytic activity of the sample. The d_{DLS} value of the highest activity sample is lower than that of P25 B. This confirmed that the level of aggregation probably has an important influence on the photocatalytic activity of the photocatalysts.

3.3. X-ray photoelectron spectroscopy

XP spectrum of two samples prepared by burner A (A-1.21-237-30 and A-1.10-237-30), three photocatalytically highly active samples prepared by burner B (B-1.24-237-30, B-1.24-355-30, B-1.24-710-30) as well as that of P 25 B were recorded (Fig. 3). Sample A-1.21-237-30 consisted mainly of spherical particles and it was characterized by relatively low photocatalytic activity

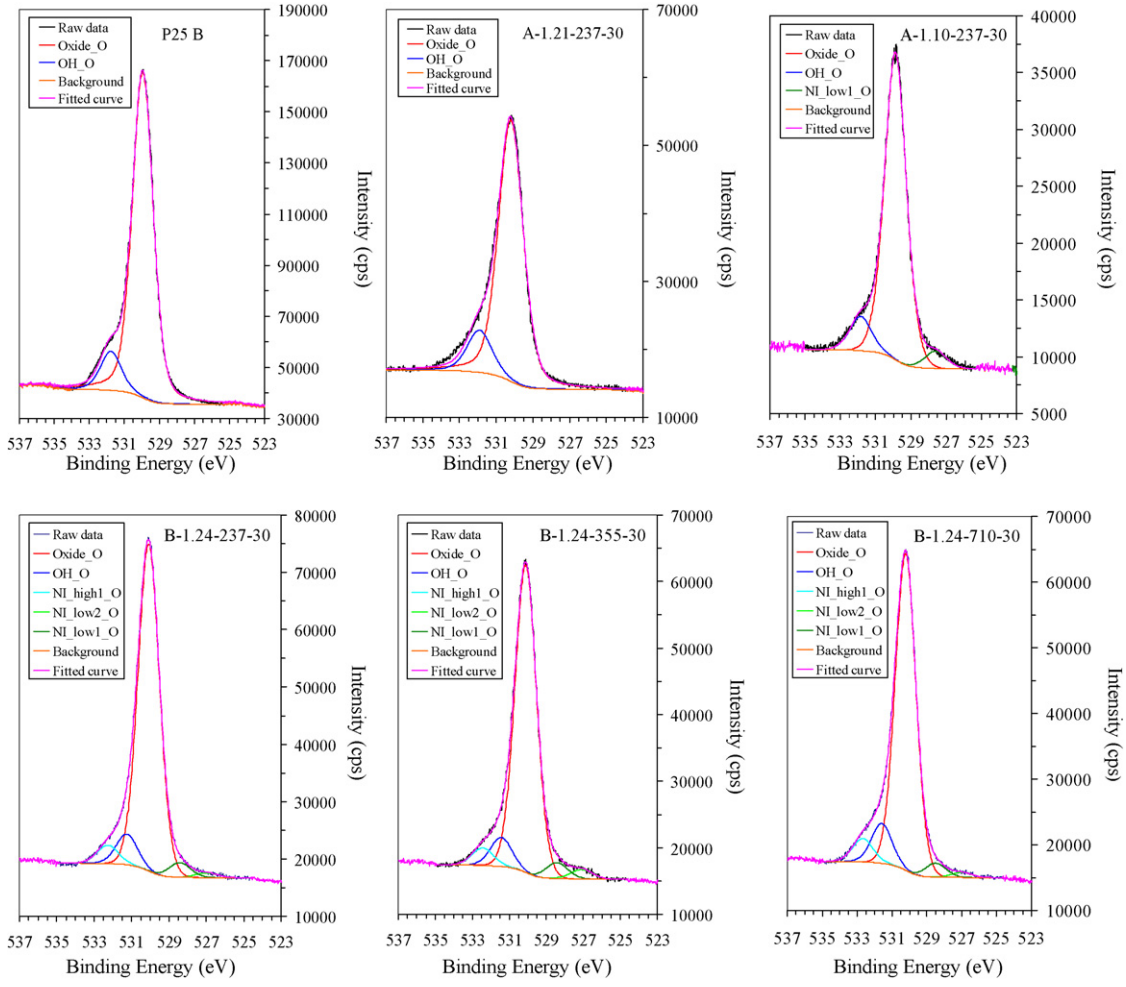

Fig. 3. O 1s XPS spectra of P25 B, a low (A-1.21-237-30) and high activity sample (A-1.10-237-30) prepared by burner A and three high activity sample prepared by burner B (NI: not indentified).

($r_{0,\text{phenol}} = 7.2 \times 10^{-8}$ M/s). Sample A-1.10-237-30 contained particles with much higher activity ($r_{0,\text{phenol}} = 17.7 \times 10^{-8}$ M/s).

The O 1s signal of the sample A-1.21-237-30 can be deconvoluted to two components: the most intense peak located at 530.2 eV is due to lattice oxygen. The one at around 531.8 eV is associated with surface OH-groups [19]. As seen in Fig. 3, similar O 1s XPS spectrum was recorded for P25 B. However, the O 1s signal of sample B-1.24-237-30 could be deconvoluted into three contributions. Besides the two peaks identified on the spectra of A-1.21-237-30 and P25 B, there is a third, least intense component located at 527.5 eV. As the O 1s signal in Ti_2O_3 is located at 529.6 eV, the peak is unlikely to correspond to this kind of O-atom. (Furthermore, from the Ti $2p_{3/2}$ XPS signal found at 459 eV for all samples characteristic to Ti^{4+}, the concentration of Ti^{3+} is negligible in the surface of the samples.)

Surprisingly, the O 1s signal of the samples prepared with burner B with high activity cannot be described with only three component peaks, in fact, five contributions had to be assumed. This means, that both on the low and high-energy sides of the lattice O-peak, further contributions appeared. The third peak on the higher binding energy side could be attributed to adsorbed water on the surface, however, the origin of the peaks on the lower binding energy side is unknown. Comparing the spectra of the last three samples made with burner B, it seems to us that these special O 1s signal features might be in correlation with the photocatalytic activity of the samples. The peaks on the lower binding energy side are more pronounced for samples with higher activity for both series. This shoulder is the most pronounced for the highest activity sample (B-1.24-355-30). We speculate that this special feature indicates so far unknown good surface properties, which possibly influence the adsorption capacity of titanium dioxide nanoparticles for water and oxygen, which are crucially important prerequisites in the photocatalytic processes when oxidizing radicals are formed.

3.4. Determination of oxygen consumption during the reaction kinetic measurements

The oxygen adsorption capacity of different titania samples was studied by Chhor et al. [35] in aqueous solutions and in water under UV irradiation. The oxygen consumption was monitored during the irradiation. Although the authors interpreted the changes observed in oxygen concentration in terms of the adsorption of oxygen on the photoexcited surface, these changes are most likely due to the oxygen consumption of the oxidation reactions involving the organic substrate.

The cell used for these experiments is shown in Fig. 4a, while on Fig. 4b some representative oxygen consumption curves for our samples and also for P25 A and B are displayed. The good reproducibility of these experiments is evident. Phenol is rapidly oxidized to aromatic dihydroxy intermediates, which further react photocatalytically with the radicals formed from the dissolved molecular oxygen, forming carboxylic acids and, finally, carbon dioxide.

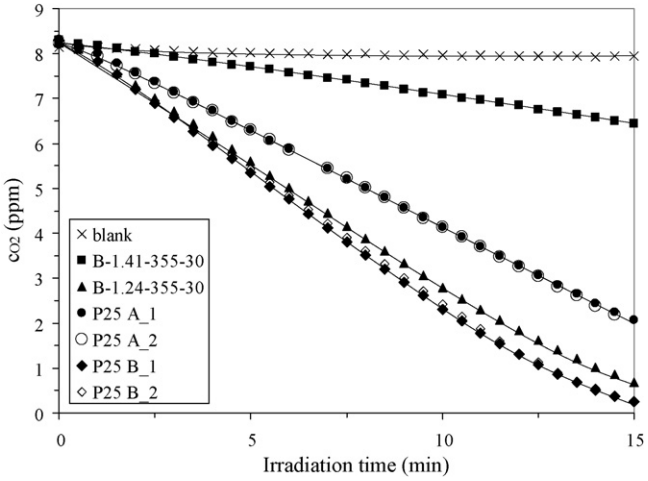

Fig. 4. (a) The photograph of the reactor used for the oxygen consumption experiments. (b) Oxygen consumption curves for P25 A and B (duplicate experiments), and for the samples with highest and lowest activity for phenol degradation determined in the traditional phenol degradation experiments (i.e., B-1.24-355-30 and B-1.41-355-30), and the blank curve (c_{phenol} = 0.5 mM, c_{TiO_2} = 1 g/L).

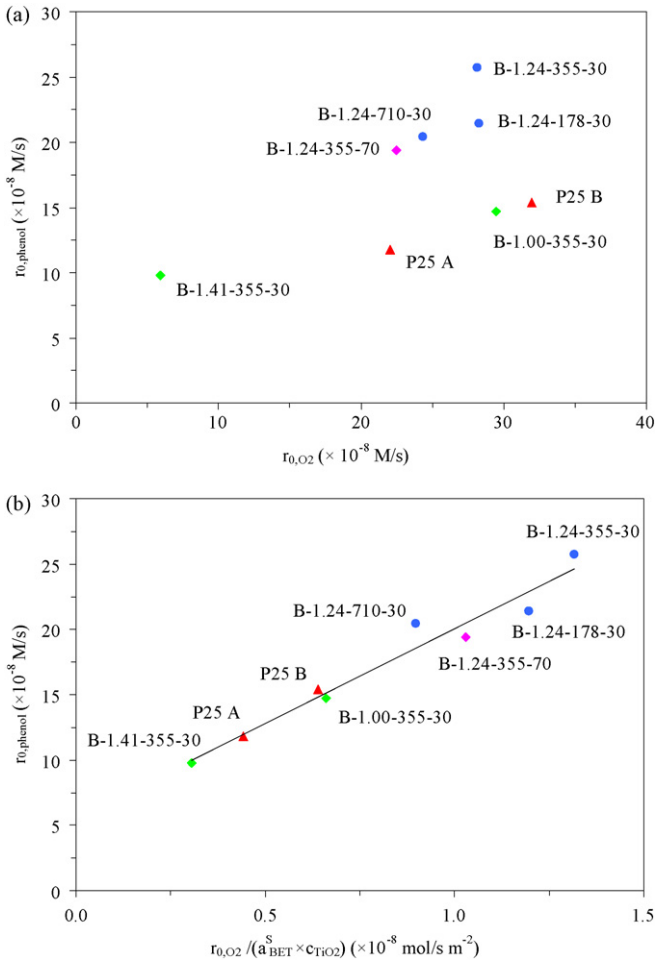

Fig. 5. (a) Initial photocatalytic degradation rate of phenol ($r_{0,phenol}$) vs. the initial photocatalytic consumption rate of oxygen (r_{0,O_2}) for the various photocatalysts studied (b) the same as (a) except, that $r_{0,O_2}/(a^{S_{BET}} \times c_{TiO_2})$ is plotted on the *X*-axis.

Since there is no oxygen supplement in the system, its concentration rapidly approaches zero. This experiment might work very well to provide well reproducible data for the comparison of the photocatalytic activity of a series of photocatalyst samples in significantly shorter time (~10–15 min) than that of conventional photocatalytic activity experiments. The experiment requires only 20 mg of the photocatalyst sample and an inexpensive instrument. Although this oxygen consumption does not reveal novel information about the mechanism of photooxidation, the slope of the oxygen consumption curve is obviously related to the photocatalytic mineralization activity of the sample for a given substrate. Since there is a short plateau at the beginning of these curves, an empirical function has been fitted on the data points between 2 and 15 min. The slope of this function at t = 2 min was calculated, and considered to be the measure of the initial consumption rate of oxygen (r_{0,O_2}).

Fig. 4b shows the oxygen consumption curves for the samples B-1.24-355-30 and B-1.41-355-30. On the basis of Table 1, these samples displayed the highest and lowest photocatalytic activities in the traditional phenol decomposition experiment. On the basis of Fig. 4b it seems that the oxygen consumption rate measured on these specimens is different, and correlates with the decomposition rate of phenol observed in traditional photocatalytic decomposition experiment. A similar kind of difference was also observed for P25 A and B [1,2] and it is also evident in this experiment.

It should be noted however that although $r_{0,phenol}$ was higher for sample B-1.24-178-30 than for P25 A and B, its r_{0,O_2} is situated between these two. Moreover, when $r_{0,phenol}$ values are plotted against r_{0,O_2} values for each sample (see Fig. 5a), no simple correlation between $r_{0,phenol}$ and r_{0,O_2} is seen. However if $r_{0,phenol}$ values are plotted against the normalized r_{0,O_2} values (i.e., $r_{0,O_2}/(a^{S_{BET}} \times c_{TiO_2})$) an interesting linear behaviour is observed. The latter (normalized) reaction rate describes the general photocatalytic quality of the surface of the photocatalyst (i.e., it gives the molar amount of converted molecular oxygen over the surface unit in a second, mol s^{-1} m^{-2}). As this quality is being improved the phenol decomposition rate also increases. This correlation suggests, that oxygen adsorption on the photocatalyst surface could be an important factor in determining photocatalytic activity, however, further studies are needed for deeper understanding of this observation.

3.5. Intermediate studies

During the photocatalytic reactions, phenol is converted into dihydroxy intermediates, such as HQ and PC. When these compounds are further oxidized, carboxylic acids and finally carbon dioxide are formed. Molecular oxygen can accept photoexcited electrons forming superoxide radicals and finally •OH radicals. Similarly, OH^- ions can react with the photoexcited holes and also

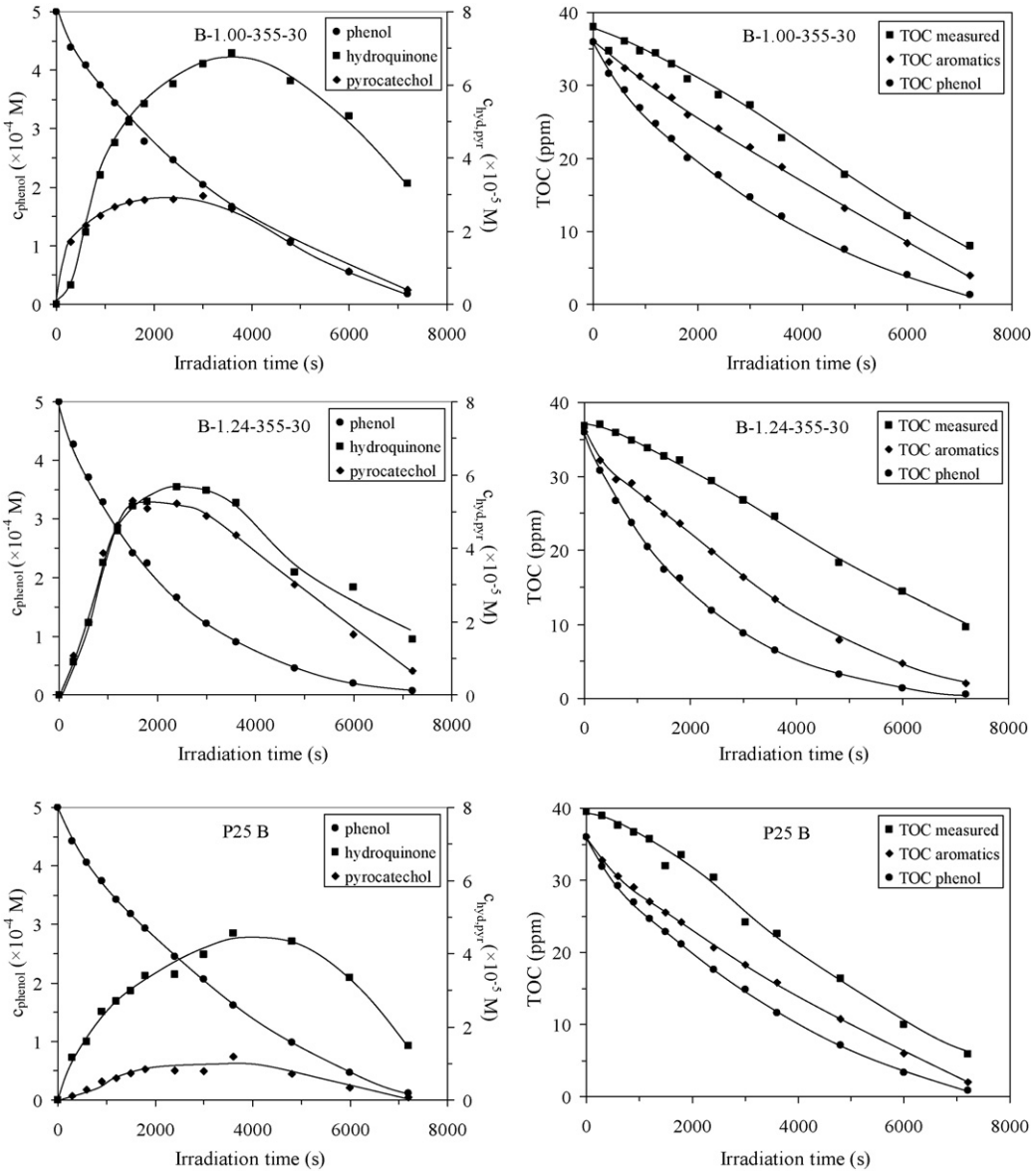

Fig. 6. Left column: decay curves of phenol and variation of the concentration of hydroquinone (HQ) and pyrocatechol (PC) during the photocatalytic decomposition of phenol using sample B-1.00-355-30, B-1.24-355-30 and P25 B. The formation of HQ and PC was monitored by HPLC. Right column: the complete mineralization was followed by measuring the total organic carbon concentration (TOC) in parallel with the HPLC analysis from the solution phase, i.e., calculated TOC contribution curves associated with the phenol content and with all the monitored aromatic intermediates (TOC phenol and TOC aromatics, respectively).

form •OH radicals. The final conclusion is that 1 mol oxygen is consumed for converting 2 moles of phenol. This means that if there were no other reaction in the system, the ratio of $r_{0,O_2}/r_{0,phenol}$ should be equal to be 0.5. Obviously, if there are other intermediates or the end product is formed in parallel process, then $r_{0,O_2}/r_{0,phenol} > 0.5$. Although the experimental conditions are not identical in our traditional photocatalytic experiments and in the oxygen consumption experiments, the $r_{0,O_2}/r_{0,phenol}$ ratio may still be informative. It can be seen from Table 2, that for our samples, $0.6 \leq r_{0,O_2}/r_{0,phenol} \leq 1.9$ (and for P25 B, $r_{0,O_2}/r_{0,phenol} = 2.05$). As we stated earlier, sample B-1.00-355-30 is very similar to P25 B; this similarity is further confirmed by the very similar $r_{0,O_2}/r_{0,phenol}$ values (1.88 and 2.05, respectively) of these two specimens.

Regarding the complete removal of toxic organics from polluted water, it is necessary to know the quality and the concentration of the intermediates formed from the primary substrate. This also may provide deeper understanding on the mechanism of the reactions occurring and could provide a better chance to select the optimal photocatalyst for a given organic target compound. Concentration profiles of intermediate are shown for three photocatalytic experiments, including B-1.00-355-30, B-1.24-355-30 and P25 B (Fig. 6). During the decomposition of phenol, two main dihydroxy intermediates, HQ and PC are formed. They reach a maximum concentration at a certain irradiation time (c_{max}^{HQ} and c_{max}^{PC} in Table 2) depending on the quality of the photocatalyst and than they are also converted to other intermediates, therefore their concentration finally goes to zero. It is obvious from Fig. 6, that the $c_{max}^{HQ}/c_{max}^{PC}$ ratio can be quite different (2.30, 1.48 and 4.40 for the samples B-1.00-355-30, B-1.24-355-30 and P25 B, respectively). These smaller numbers are mainly due to the formation of more PC compared to the suspension containing P25 B. Its concentration was found to be 2–4× greater compared to the case of P25 B. PC is known to be an efficiently chemisorbing substrate on titanium dioxide. Specific surface areas of our samples are smaller than that of P25 B, therefore PC cannot be adsorbed as efficiently on our samples as on the P25 B particles. Because the chemisorbed fraction is rapidly oxidized further,

such intermediates are more efficiently oxidised on P25 B than on our catalysts. Similar change was noticed in one of our earlier publication with fluorinated titanias [7]. On the fluorinated particles, the density of OH-groups is reduced, the adsorption of PC is also hindered. Although the highest concentration of these intermediates is about one magnitude lower compared to the concentration of phenol, this effect also may further increase the activity of our photocatalysts for phenol decomposition.

Total organic carbon analysis was also carried out in these systems. Fig. 6 reveals the complete mineralization of phenol on the basis of the TOC observed vs. time curves. In order to help the comparison among these samples, a TOC value was also calculated for the phenol content (TOC phenol) and for the sum of the aromatic intermediates identified (including phenol, TOC aromatics) based on the data collected by the HPLC measurements. TOC values decrease efficiently in all three systems indicating that these are all good photocatalysts for the complete purification of polluted water. It is easily observable that the difference between TOC measured and TOC aromatics is larger for sample B-1.24-355-30 compared to the other two similar systems. This difference tells us about the presence of non aromatic intermediates (such as carboxylic acids), which are more readily decomposed on photocatalysts with higher specific surface area (i.e., P25 B). Based on these observations, one might like to select either the best quality photocatalyst for removing the most toxic phenol as fast as possible (i.e., specimen B-1.24-355-30 is chosen), or provide the highest rate for the total mineralization of organics present in contaminated water (i.e., P25 B is selected).

4. Conclusions

The present publication deals with the surface properties of polyhedral flame made titanium dioxide photocatalysts. The aggregation of titania nanoparticles could have an important influence on their photocatalytic activity. If other parameters are almost identical (such as polyhedrality, particle size and phase composition), the particles with the highest hydrophilicity are the best photocatalysts for the degradation of poorly adsorbing model substrates. This was confirmed in our experiments with the highest activity sample owning one of the smallest aggregate sizes in solutions. Oxygen consumption experiments were found to be well reproducible, fast and inexpensive measurements for the determination of the photocatalytic activity of the prepared photocatalysts. After normalization with the specific surface area and the concentration of the suspension, such simple experiments are also capable of describing the overall goodness of the catalyst surface for the mineralization of a given substrate. For the selection of the optimal synthesis parameters, it has to be taken into consideration whether the main goal is the removal of a given compound as fast as possible (irrespective of the further decomposition rate of the primary decomposition products), or the complete mineralization of the target substrate. Our work proved, that for the first case polyhedral titania particles with moderately low specific surface area ($\sim$20 m^2/g) can be recommended, while in the latter case polyhedral particles with medium specific surface area ($\sim$50 m^2/g) are the best, such as P25 B TiO_2.

Acknowledgements

KM thanks the Magyary Zoltán Foundation for the kind financial support. This work was financially supported by grants from the Hungarian National Office of Research and Technology (NKFP DA_THERM TECH_08_A4), the Hungarian Research Foundation (OTKA grants no. 67559 and 78378) and the bilateral Hungarian-Romanian TeT cooperation project (OMFB-00415/2008/RO-21/2007).

References

[1] N. Balázs, K. Mogyorósi, D.F. Srankó, A. Pallagi, T. Alapi, A. Oszkó, A. Dombi, P. Sipos, Appl. Catal. B 84 (2008) 356–362.
[2] N. Balázs, D.F. Srankó, A. Dombi, P. Sipos, K. Mogyorósi, Appl. Catal. B, submitted for publication.
[3] J. Ryu, W. Choi, Environ. Sci. Technol. 42 (2008) 294–300.
[4] K. Mogyorosi, A. Farkas, I. Dekany, I. Ilisz, A. Dombi, Environ. Sci. Technol. 36 (2002) 3618–3624.
[5] I. Ilisz, A. Dombi, K. Mogyorósi, A. Farkas, I. Dékány, Appl. Catal. B 39 (2002) 247–256.
[6] I. Ilisz, A. Dombi, K. Mogyorósi, I. Dékány, Colloids Surf. A 230 (2003) 89–97.
[7] P. Calza, E. Pelizzetti, K. Mogyorósi, R. Kun, I. Dékány, Appl. Catal. B 72 (2007) 314–321.
[8] A. Piscopo, D. Robert, J.V. Weber, J. Photochem. Photobiol. A 139 (2001) 253–256.
[9] Y. Zhao, C. Li, X. Liu, F. Gu, J. Alloys Compd. 440 (2007) 281–286.
[10] K.K. Akurati, A. Vital, G. Fortunato, R. Hany, F. Nueesch, T. Graule, Solid State Sci. 9 (2007) 247–257.
[11] C.B. Almquist, P. Biswas, J. Catal. 212 (2002) 145–156.
[12] R. Kavitha, S. Meghani, V. Jayaram, Mater. Sci. Eng. B 139 (2007) 134–140.
[13] R. Hong, Z. Rena, J. Ding, H. Li, Chem. Eng. J. (Amsterdam, Neth.) 108 (2005) 203–209.
[14] A. Teleki, R. Wengeler, L. Wengeler, H. Nirschl, S.E. Pratsinis, Powder Technol. 181 (2008) 292–300.
[15] K.K. Akurati, A. Vital, U.E. Klotz, B. Bommer, T. Graule, M. Winterer, Powder Technol. 165 (2006) 73–82.
[16] Y. Zhao, C. Li, X. Liu, F. Gu, H.L. Du, L. Shi, Appl. Catal. B 79 (2008) 208–215.
[17] Y. Zhao, C. Li, X. Liu, F. Gua, H.L. Duc, L. Shi, Mater. Chem. Phys. 107 (2008) 344–349.
[18] W.Y. Teoh, R. Amal, L. Madler, S.E. Pratsinis, Catal. Today 120 (2007) 203–213.
[19] S. Ardizzone, C.L. Bianchi, G. Cappelletti, S. Gialanella, C. Pirola, V. Ragaini, J. Phys. Chem. C 111 (2007) 13222–13231.
[20] X.J. Li, J.W. Cubbage, T.A. Tetzlaff, W.S. Jenks, J. Org. Chem. 64 (1999) 8509–8524.
[21] X.J. Li, J.W. Cubbage, W.S. Jenks, J. Org. Chem. 64 (1999) 8525–8536.
[22] A. Mills, J.S. Wang, J. Photochem. Photobiol. A 118 (1998) 53–63.
[23] U. Stafford, K.A. Gray, P.V. Kamat, J. Catal. 167 (1997) 25–32.
[24] J. Theurich, M. Lindner, D.W. Bahnemann, Langmuir 12 (1996) 6368–6376.
[25] J.C. D'Oliveira, G. Al-Sayyed, P. Pichat, Environ. Sci. Technol. 24 (1990) 990–996.
[26] L. Rideh, A. Wehrer, D. Ronze, A. Zoulalian, Ind. Eng. Chem. Res. 36 (1997) 4712–4718.
[27] Y. Ku, R.M. Leu, K.C. Lee, Water Res. 30 (1996) 2569–2578.
[28] I. Ilisz, A. Dombi, Appl. Catal. A 180 (1999) 35–45.
[29] A. Dombi, I. Ilisz, Zs. László, Gy. Wittmann, Ozone: Sci. Eng. 24 (2002) 49–54.
[30] Z. Ambrus, K. Mogyorósi, Á. Szalai, T. Alapi, K. Demeter, A. Dombi, P. Sipos, Appl. Catal. A 340 (2008) 153–161.
[31] G. Dagan, M. Tomkiewicz, J. Phys. Chem. 97 (1993) 12651–12655.
[32] Y. Xie, C. Yuan, J. Mol. Catal. A: Chem. 206 (2003) 419–428.
[33] S.J. Kim, E.G. Lee, S.D. Park, C.J. Jeon, Y.H. Cho, C.K. Rhee, W.W. Kim, J. Sol–Gel Sci. Technol. 22 (2001) 63–71.
[34] H. Kominami, H. Kumamoto, Y. Kera, B. Ohtani, J. Photochem. Photobiol. A 160 (2002) 99–104.
[35] K. Chhor, J.F. Bocquet, C. Colbeau-Justin, Mater. Chem. Phys. 86 (2004) 123–131.
[36] D. Gumy, S.A. Giraldo, J. Rengifo, C. Pulgarin, Appl. Catal. B 78 (2008) 19–29.
[37] R.J. Hunter, Zeta Potential in Colloid Science, Principles and Applications, Academic Press, London, 1981, p. 386.
[38] M. Kosmulski, Adv. Coll. Int. Sci. 99 (2002) 255–264.